Kinetics and Mechanism of the Monomerization of a Re(V) Dithiolato Dimer with Monodentate Ligands. Electronic and Steric Effects

Gábor Lente, Ilia A. Guzei, and James H. Espenson*

Ames Laboratory and Department of Chemistry, Iowa State University of Science and Technology, Ames, Iowa 50011

Received December 15, 1999

The sulfur-bridged dimeric dithiolato rhenium(V) chelate $[CH_3(O)Re(\eta^2,\mu\text{-o-}SCH_2C_6H_4S)]_2$ (**D**), derived from 2-mercaptothiophenol, was monomerized to give $[CH_3(O)Re(\eta^2\text{-o-}SCH_2C_6H_4S)]$**L** (**M**−**L**) in benzene upon reaction with various neutral and anionic monodentate ligands (**L**) such as pyridine and its substituted derivatives, triarylphosphines, dimethyl sulfoxide, 4-picoline-*N*-oxide, and halide ions. The kinetic observations can readily be interpreted for all ligands by a unified mechanism in which the initial fast formation of a 1:1 (**DL**) and 1:2 ($\mathbf{DL_2}$) adduct is followed by the slow monomerization of each species so formed. The use of different ligands gave insight into different steps of the same multistep mechanism. The kinetics of ligand exchange between free **L** and the monomeric complexes was also studied; an associative pathway has been proposed to interpret the results. The crystal structures of two new monomeric **ML** complexes (with **L** = 4-acetylpyridine and 1,3-diethylthiourea) are reported.

Introduction

Methyltrioxorhenium(VII) (CH_3ReO_3, abbreviated as MTO) is a versatile catalyst. It is air- and water-stable, and soluble in a large variety of solvents in which it can be used in a number of useful transformations.[1−4] In one group of reactions MTO is used to catalyze oxidations by hydrogen peroxide. In another, it catalyzes various atom-transfer reactions from a donor to an acceptor. In this second group of reactions, lower oxidation-state rhenium intermediates, most notably those of Re(V), have been postulated from kinetics evidence and sometimes detected.[5,6] Recent work on the MTO-catalyzed stereospecific desulfurization of thiiranes[7] focused our attention on thiolato rhenium(V) complexes in which the rhenium−carbon bond remains fully intact. Reaction of MTO with the chelating ligand l,2-mercaptothiophenol in toluene gave a sulfur-bridged dithiolato methyloxorhenium(V) dimer (designated here as **D**):[8]

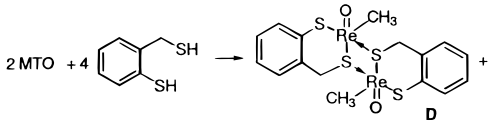

(1)

Our principal objective has been to characterize the reactivity of the dimer **D** because such studies may further enlighten certain mechanistic aspects of MTO-catalyzed atom-transfer reactions. **D** can be monomerized readily with various ligands, giving Re(V) complexes having a monodentate ligand in addition to the chelating dithiolato ligand.

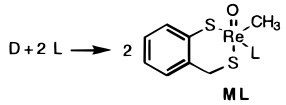

(2)

In this paper we report detailed studies of the kinetics and mechanism of the monomerization reaction with a series of ligands and of exchange reactions between the free ligands and the **ML** complexes. This includes the results of kinetics and equilibrium experiments, X-ray crystallography, and matrix rank analysis for the determination of the number of species present.

Experimental Section

Materials. MTO was synthesized from sodium perrhenate and tetramethyltin (Strem) according to the procedure published earlier.[9] 2-Mercaptomethylthiophenol[10,11] and the dimer **D**[8] were synthesized as described earlier. Other reagents, including substituted pyridines (Aldrich) and triphenylphosphines (Strem), were purchased from commercial sources and used without further purification except for 4-pyridinecarboxaldehyde that was distilled in a vacuum and handled under argon. Benzene (Fisher spectraanalyzed) was used as a solvent throughout this study. Unless otherwise stated, the rate constants reported in this paper were determined at 25.0 °C.

(1) Romão, C. C.; Kühn, F. E.; Herrmann, W. A. *Chem. Rev.* **1997**, *97*, 3197−3246.
(2) Conry, R. R.; Mayer, J. M. *Inorg. Chem.* **1990**, *29*, 4862−4867.
(3) Espenson, J. H. *Chem. Commun* **1999**, 479−488.
(4) Espenson, J. H.; Abu-Omar, M. M. *Adv. Chem. Ser.* **1997**, *253*, 99−134.
(5) Abu-Omar, M. M.; Appelmann, E. H.; Espenson, J. H. *Inorg. Chem.* **1996**, *35*, 7751−7757.
(6) Abu-Omar, M. M.; Espenson, J. H. *Inorg. Chem.* **1996**, *34*, 6239−6240.
(7) Jacob, J.; Espenson, J. H. *Chem. Commun.* **1999**, 1003−1004.
(8) Jacob, J.; Guzei, I. A.; Espenson, J. H. *Inorg. Chem.* **1999**, *38*, 1040−1041.
(9) Herrmann, W. A.; Kratzer, R. M.; Fischer, R. W. *Angew. Chem., Int. Ed. Engl.* **1997**, *36*, 2652−2654.
(10) Klingsberg, E.; Screiber, A. M. *J. Am. Chem. Soc.* **1962**, *84*, 2941−2944.
(11) Hortmann, A. G.; Aron, A. J.; Bhattacharya, A. K. *J. Org. Chem.* **1978**, *43*, 3374−3378.

10.1021/ic991431p CCC: $19.00
Published on Web 03/01/2000

Instrumentation. Shimadzu scanning spectrophotometers and a Shimadzu Multispec 1501 diode-array spectrophotometer were used to record UV−vis spectra and kinetic curves. A 1 cm cell was used except for the study with tetrabutylammonium iodide where its low solubility required much lower concentrations and a 10 cm cell. An Applied Photophysics DX-17 MV sequential stopped−flow apparatus was used in single mixing mode for fast reactions. The optical path length in the stopped−flow instrument was 1 cm. In every kinetics experiment (stopped−flow and conventional UV−vis) the measured initial absorbances were compared with corresponding blank curves, in which one of the reagents was absent, to detect possible reactions occurring in the mixing time. Single-wavelength kinetic studies for the monomerization reactions were usually run at 610 nm, where all the **ML** complexes have considerable absorption and **D** absorbs very little. Kinetics data for the ligand exchange reactions were evaluated at ∼400 nm to obtain the maximum absorbance change.

^{1}H NMR spectra were recorded with Varian VXR 300 MHz and Bruker DRX 400 MHz spectrometers. The ^{1}H chemical shifts were measured relative to the residual ^{1}H resonance of the deuterated solvent C_6D_6 ($\delta = 7.16$ ppm). Because all the reactions were accompanied by substantial UV−vis spectral changes, the NMR technique was used only to monitor reactions qualitatively and to identify the products.

Computation. Stopped−flow kinetics curves were fitted with the nonlinear least-squares routine in the software package provided by the manufacturer. Each rate constant was determined as the average of at least five values from replicate kinetic runs and was reproducible within 5%. The software PSEQUAD[12] was used to obtain equilibrium constants from multiwavelength absorbance data. These calculations are based on the net absorbance change from beginning to end and are independent of the kinetic measurements. Typically, absorbance readings were recorded at 25−35 different wavelengths in the 320−700 nm range; this set of values was used in a global fit to extract the equilibrium constant for each pyridine derivative. The concentration ranges were $[Re]_T = 0.2-2$ mmol L^{-1} and $[L]_T = 2-800$ mmol L^{-1} and were designed for each individual ligand specifically to optimize the precision of equilibrium measurements.

Rate constants from spectrophotometric experiments were obtained by nonlinear least-squares fitting. Linearized forms were used only to visualize data. The method of flooding was used whenever applicable, and the functional dependence of the pseudo-first-order rate constants on the concentration of the reagent in excess was used to derive the rate law. With a few ligands, multiwavelength kinetic data were fitted simultaneously in a global fit to determine pseudo-first-order rate constants. That is, from data at n wavelengths, one obtains from this method a single k_{obs}, n amplitudes ($Abs_0 - Abs_\infty$), and n end points (Abs_∞).[13]

Calculations for matrix rank analysis[14] were carried out by the software MRA.[15] This method was used to determine the minimum number of absorbing species from UV−vis spectral data based on the singular values of the data matrix. An example of this process is given in the Supporting Information.

Isolation and Crystallographic Parameters of M−L, L = 4-Acetylpyridine, $C_{15}H_{16}NO_2ReS_2$. Preparation. To 3 mg of **D** dissolved in 2 mL of benzene was added 30 μL of 4-acetylpyridine. The color of the solution turned a bright greenish-yellow in about 15 min. The product was isolated in crystalline form with slow diffusion of hexane into the solution. X-ray crystal data: monoclinic, $P2_1/c$, $a = 16.8291(9)$ Å, $b = 7.4348(4)$ Å, $c = 12.9117(7)$ Å, $\beta = 98.710(1)°$, $V = 1596.89(15)$ Å^3, $Z = 4$, $T = 173(2)$ K, $D_{calc} = 2.049$ Mg/m^3, $R(F) = 2.34\%$ for 3761 independently observed ($I \geq 2\sigma(I)$) reflections ($4° \leq 2\theta \leq 57°$).

Isolation and Crystallographic Parameters of M−L, L = 1,3-Diethylthiourea, $C_{13}H_{21}N_2ORS_3$. Preparation. To 3 mg of **D** dissolved in 2 mL of benzene was added 100 μL of ethyl isothiocyanate, which is known to react with moisture giving 1,3-diethylthiourea. The solution was stored at room temperature; after 1 month crystals formed. X-ray crystal data: monoclinic, $C2/c$, $a = 26.5431(13)$ Å, $b = 9.4650(5)$ Å, $c = 15.6416(7)$ Å, $\beta = 117.385(1)°$, $V = 3489.3(3)$ Å^3, $Z = 8$, $T = 173(2)$ K, $D_{calc} = 1.918$ Mg/m^3, $R(F) = 1.93\%$ for 3555 independently observed ($I \geq 2\sigma(I)$) reflections ($4° \leq 2\theta \leq 53°$).

Crystallography. The crystal evaluation and data collection were performed using a Bruker CCD-1000 diffractometer with Mo Kα ($\lambda = 0.710\,73$ Å) radiation. The diffractometer-to-crystal distance was 5.08 cm. All atoms other than hydrogen were refined with anisotropic displacement coefficients. All hydrogen atoms were included in the structure factor calculation at idealized positions and were allowed to ride on the neighboring atoms with relative isotropic displacement coefficients. The software and sources of the scattering factors are contained in the SHELXTL (version 5.1) program library.[16] Absorption corrections were carried out by programs SADABS.[17]

Chart 1

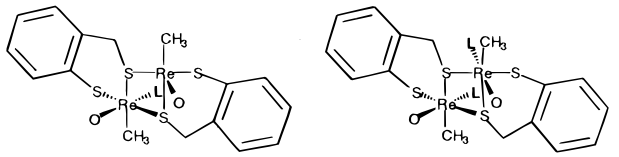

DL **DL$_2$**

Results

Preliminary Considerations. The monomerization of **D** is believed to occur via two intermediates, **DL** and **DL$_2$**, the suggested structures of which are given in Chart 1. The following scheme was proposed earlier to interpret monomerization reactions with pyridine and triphenylphosphine:[18,19]

$$\mathbf{D} + \mathbf{L} \underset{k_{-1}}{\overset{k_1}{\rightleftharpoons}} \mathbf{DL} \tag{3}$$

$$\mathbf{DL} + \mathbf{L} \underset{k_{-2}}{\overset{k_2}{\rightleftharpoons}} \mathbf{DL_2} \tag{4}$$

$$\begin{array}{l} \mathbf{DL} + \mathbf{L} \underset{k_{-2}}{\overset{k_2}{\rightleftharpoons}} \mathbf{DL_2} \\ \mathbf{DL} \xrightarrow{k_3} \mathbf{ML} + \mathbf{M} \\ \qquad\qquad \xrightarrow[\text{fast}]{+\,\mathbf{L}} \mathbf{ML} \end{array} \tag{5}$$

$$\mathbf{DL_2} \xrightarrow{k_4} 2\mathbf{ML} \tag{6}$$

This scheme has been able to account for all of the monomerization reactions studied. Let us assume that reactions 3 and 4 are rapidly established equilibria in all instances because that has been shown to be the case directly for every case in which **DL** or **DL$_2$** was formed in detectable amounts. With that assumption, then one can derive the following rate law for experiments done with a large excess of ligand:

$$-\frac{\mathrm{d}[\mathbf{D}]}{\mathrm{d}t} = \frac{1}{2}\frac{\mathrm{d}[\mathbf{ML}]}{\mathrm{d}t} = \frac{k_3K_1[\mathbf{L}] + k_4K_1K_2[\mathbf{L}]^2}{1 + K_1[\mathbf{L}] + K_1K_2[\mathbf{L}]^2}[\mathbf{D}] \tag{7}$$

where the parameters are those given in eq 3−6, with $K_1 =$

(12) Zékány, L.; Nagypál, I. In *Computational Methods for the Determination of Formation Constants*; Legett, D. J., Ed.; Plenum Press: New York, 1985; pp 291−299.
(13) *Scientist*, version 2.0; Micromath Software, 1995.
(14) Peintler, G.; Nagypál, I.; Jancsó, A.; Epstein, I. R.; Kustin, K. *J. Phys. Chem. A* **1997**, *101*, 8013−8020.
(15) Peintler, G. version 3.04; Attila József University: Szeged, 1997.
(16) Sheldrick, G. *Brüker Analytical X-ray Systems*; Madison, WI,.
(17) Blessing, R. H. *Acta Crystallogr.* **1995**, *A51*, 33−38.
(18) Jacob, J.; Lente, G.; Guzei, I. A.; Espenson, J. H. *Inorg. Chem.* **1999**, *38*, 3762−3763.
(19) Lente, G.; Jacob, J.; Guzei, I. A.; Espenson, J. H. *Inorg. React. Mech.*, in press.

Table 1. Kinetic and Equilibrium Data for Monomerization with Pyridine Derivatives at 25.0 °C in Benzene

	σ	K_D/L mol^{-1}	k_b/L^2 mol^{-2} s^{-1}	k_a/L mol^{-1} s^{-1}
4-$Me_2NC_5H_4N$	−0.83	$>5 \times 10^4$ [c]	$(6.41 \pm 0.03) \times 10^4$	$<6 \times 10^1$ [a]
4-methoxypyridine	−0.27	$(4.0 \pm 0.1) \times 10^3$	$(3.76 \pm 0.05) \times 10^2$	$<5 \times 10^0$ [a]
4-*tert*-butylpyridine	−0.20	$(4.07 \pm 0.09) \times 10^3$	$(9.7 \pm 0.3) \times 10^1$	$<2 \times 10^0$ [a]
4-picoline	−0.17	$(1.00 \pm 0.05) \times 10^3$	$(1.33 \pm 0.02) \times 10^2$	$<3 \times 10^0$ [a]
3-picoline	−0.07	$(1.07 \pm 0.02) \times 10^3$	$(6.19 \pm 0.06) \times 10^1$	$<1 \times 10^0$ [a]
4-phenylpyridine	−0.01	$(1.15 \pm 0.03) \times 10^3$	$(7.0 \pm 0.06) \times 10^1$	$<1 \times 10^0$ [a]
pyridine	0.00	$(1.74 \pm 0.04) \times 10^2$	$(1.31 \pm 0.03) \times 10^1$	$<3 \times 10^{-1}$ [a]
3-phenylpyridine	0.06	$(8.9 \pm 0.2) \times 10^1$	$(7.3 \pm 0.5) \times 10^0$	$(1.1 \pm 0.3) \times 10^{-1}$
3-chloropyridine	0.37	$(2.5 \pm 0.2) \times 10^{-1}$	$(7.7 \pm 0.1) \times 10^{-2}$	$(4.0 \pm 1.0) \times 10^{-3}$
4-pyridinecarboxaldehyde	0.45	$(8.9 \pm 0.8) \times 10^0$	$(3.3 \pm 0.4) \times 10^{-1}$	$(2.7 \pm 0.2) \times 10^{-2}$
4-acetylpyridine	0.50	$(1.2 \pm 0.2) \times 10^1$	$(1.5 \pm 0.1) \times 10^0$	$(4.9 \pm 0.5) \times 10^{-2}$
3-cyanopyridine	0.56	$\sim 3 \times 10^{-3}$	$(2.9 \pm 0.2) \times 10^{-3}$	$(4.3 \pm 0.8) \times 10^{-4}$
4-cyanopyridine	0.66	$(1.9 \pm 0.2) \times 10^{-1}$	$(2.7 \pm 0.2) \times 10^{-2}$	$(2.8 \pm 0.7) \times 10^{-3}$
pyrazine	*b*	$(1.3 \pm 0.1) \times 10^{-1}$	$(2.5 \pm 0.8) \times 10^{-2}$	$(3.3 \pm 0.5) \times 10^{-3}$
4-methylthiazole	*b*	$(2.2 \pm 0.2) \times 10^{-2}$	$(1.9 \pm 0.3) \times 10^{-3}$	$(1.5 \pm 0.1) \times 10^{-3}$
2-picoline	*b*	$\sim 1 \times 10^{-2}$	*a*	$(9.0 \pm 0.1) \times 10^{-3}$

[a] Too small to be determined reliably. [b] Not defined. [c] Practically complete reaction.

k_1/k_{-1} and $K_2 = k_2/k_{-2}$. Over any particular range of ligand concentration, this equation gives rise to a number of limiting rate laws depending on the particular values of equilibrium and rate constants that are dominant. These forms are of considerable use in resolving certain steps in the reaction scheme; the concept of these limiting rate laws will be elaborated in the following sections.

L = Pyridine. The reaction between **D** and pyridine produces the indicated monomeric product, the crystal structure of which was reported earlier.[19] In solution, however, this reaction does not proceed to completion. With both NMR and UV−vis detection, an increase in pyridine concentration caused more monomer to form. A series of experiments was carried out with various pyridine derivatives containing substituents in the 3 or 4 position. Both types of data were consistent with reaction 2 being an equilibrium characterized by the equilibrium constant K_D.

$$K_D = \frac{[\mathbf{M}-\mathbf{L}]^2}{[\mathbf{D}][\mathbf{L}]^2} \tag{8}$$

The equilibrium constants so determined are listed in Table 1.

With the exception of **L** = 4-(dimethylamino)pyridine, considered later, the following expression proved applicable to each of the pyridine ligands. It expresses the rate of the forward reaction in terms of concentrations:

$$v_f = \{k_a[\mathbf{L}] + k_b[\mathbf{L}]^2\}[\mathbf{D}] \tag{9}$$

This rate law is a limiting form of eq 7 applicable when $K_1[\mathbf{L}] + K_1K_2[\mathbf{L}]^2 \ll 1$, the conditions under which the concentrations of the complexes **DL** and **DL$_2$** remain much lower than that of **D** throughout the reaction. Comparison of eqs 7 and 9 yields $k_a = k_3K_1$ and $k_b = k_4K_1K_2$. These composite constants cannot be further resolved for the pyridine derivatives without an independent evaluation of K_1 and K_2.

For the more reactive pyridine derivatives (X = 3-Me, 4-Ph, 4-MeO, 4-*t*-Bu, 4-Me, and H) k_a was too small to be determined reliably; thus, the overall third-order term dominated in the rate law.

The least reactive pyridine derivatives (X = 3-CN, 4-CN, 3-Cl, 4-CHO) did not allow the use of a ligand in high enough concentration to shift the equilibrium of reaction 2 to completion. Also, in these cases the absorbance−time data did not adhere to pseudo-first-order kinetics. In these cases the rate law requires the inclusion of a term for the reversion reaction. Then

$$\frac{d[\mathbf{D}]}{dt} = -k_{obs+}[\mathbf{D}] + k_{obs-}[\mathbf{M}-\mathbf{L}]^2 \tag{10}$$

in which k_{obs+} and k_{obs-} are the respective pseudo-*n*th-order rate constant for the reaction in either direction. The resulting differential equation was solved exactly with a method similar to that derived by King.[20] The solution was converted to absorbance readings:

$$Abs_t = Abs_\infty + \frac{(1+q)[Abs_0 - Abs_\infty]\, e^{-k_{eq}t}}{1 + q\, e^{-k_{eq}t}} \tag{11}$$

where Abs_0 is the initial absorbance and Abs_∞ the final absorbance. The rate constant k_{eq} represents the value for the approach to equilibrium and was determined along with q from least-squares fitting to eq 11. The other two constants can be expressed in terms of k_{eq} as

$$k_{eq} = k_{obs+} + 4k_{obs-}[\mathbf{M}-\mathbf{L}]_\infty,$$

$$q = \frac{4k_{obs-}[\mathbf{M}-\mathbf{L}]_\infty}{2k_{obs+} + 4k_{obs-}[\mathbf{M}-\mathbf{L}]_\infty} \tag{12}$$

Thus, a straightforward combination of the determined parameters gave k_{obs+}:

$$k_{obs+} = k_{eq}\frac{1-q}{1+q} \tag{13}$$

The measured kinetic curves were fitted to eq 11. The quantity k_{obs+} holds the same significance that k_{obs} does for complete reactions (see Supporting Information for further details). This treatment was preferred over the alternative where one fits only the last portion of the kinetic curves with an exponential function to determine an equilibration rate constant because the method outlined afforded direct information on the forward rate constants derived from data over the full time course of the experiment.

The results for all derivatives are summarized in Table 1. The values of the determined equilibrium constants K_D span a remarkably broad range, >6 orders of magnitude. Reliable determinations throughout this broad range were possible because of the second-order dependence on ligand concentration and the excellent solubility of the pyridines in benzene. A linear

(20) King, E. L. *Int. J. Chem. Kinet.* **1982**, *14*, 1285−1286.

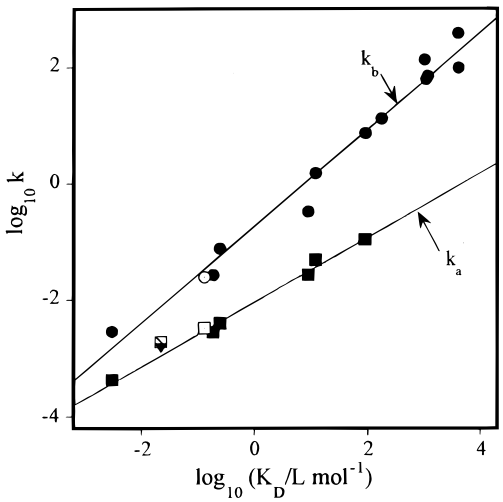

Figure 1. Linear free energy plot for monomerization of **D** with ring-substituted pyridines. Shown are values of k_a and k_b, eq 9, against K_D for eqs 2 and 8, all on logarithmic scales. Rate and equilibrium constants were determined in benzene at 25.0 °C: (■) k_a; (●) k_b; (□) pyrazine k_a; (○) pyrazine k_b; (▨) 2-methylthiazole k_a; (◇) 2-methylthiazole k_b. Slopes of straight lines are 0.55 ± 0.03 (k_a) and 0.83 ± 0.04. (k_b).

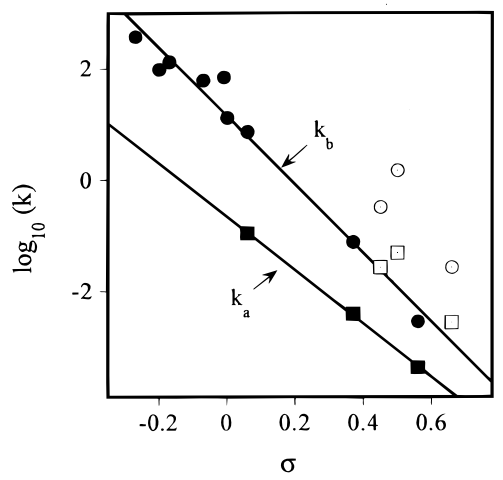

Figure 2. Hammett plot (log k_a and log k_b, eq 9, as squares and circles, respectively) against the substituent constant σ for the kinetics of monomerization of **D** with ring-substituted pyridines. Rate constants were determined in benzene at 25.0 °C.

free energy plot for the monomerization reaction 2 is shown in Figure 1, which presents log k vs log K_D. All the points for 3 and 4-substituted pyridine derivatives are on the lines, including those that deviated in the Hammett treatment, next described.

A second approach was in terms of Hammett plots for the equilibrium and rate constants, shown in Figures 2 and 3. Of the 12 data, 9 define straight lines. Three points, those for 4-acetyl, 4-formyl, and 4-cyano derivatives, deviate significantly from the straight line fitted to the remaining derivatives. The slopes of the Hammett plots, neglecting these three for the present, give the reaction constants $\rho = -4.80$ for k_a, -6.09 for k_b, and -7.51 for K_D with correlation coefficients of 0.9997, 0.984, and 0.987. These values of ρ imply a large electronic effect on the reaction. The deviations in the Hammett plot are not likely to be a consequence of a mechanism change, however, since the plots of log k vs log K_D are linear with these three data included.

The monomeric complexes **ML** with **L** = 4-acetylpyridine, 4-pyridinecarboxaldehyde, and 4-cyanopyridine (the deviating points on the Hammett plot) were bright greenish-yellow, significantly different from the usual green color of pyridine

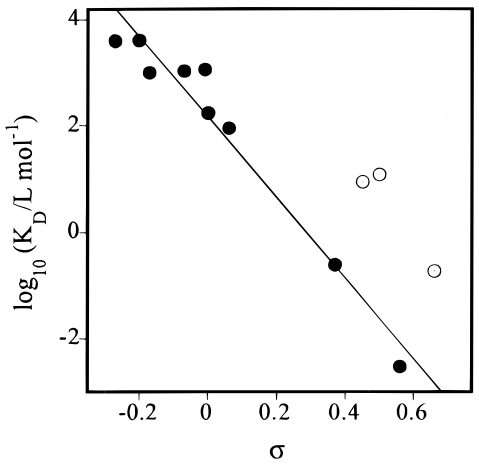

Figure 3. Hammett plot for the equilibrium between **D** and **M** with ring-substituted pyridines. Equilibrium constants were determined by UV−vis spectrophotometry in benzene at 25.0 °C. The three substituents that lie off the correlation in this plot are the same three that deviate from the lines in Figure 2.

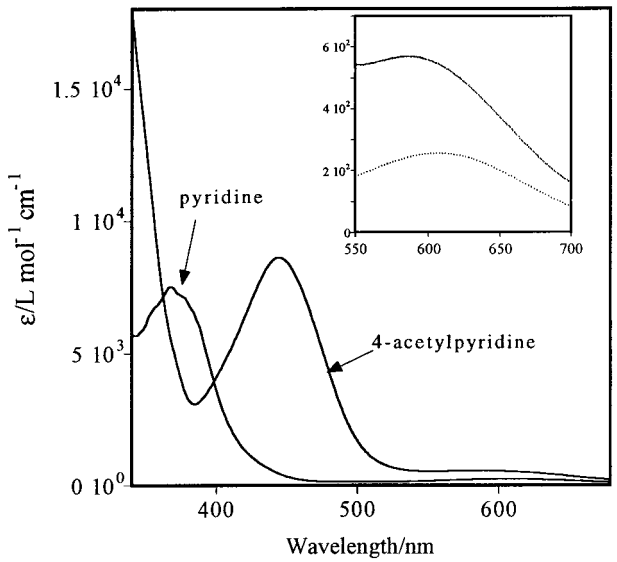

Figure 4. UV−vis spectra for two monomeric **ML** complexes, with **L** = pyridine and 4-acetylpyridine in benzene at 25.0 °C.

monomers. The UV−vis spectra of the pyridine and 4-acetylpyridine monomers are given in Figure 4 as an example. For the 4-acetylpyridine monomer, values of λ_{max}/nm (ϵ/L mol^{-1} cm^{-1}) are 444 (8620) and 586 (569); for the pyridine monomer, they are 368 (7540) and 608 (256). The monomeric adduct with 4-acetylpyridine was crystallized and its structure determined by X-ray crystallography to learn whether the different color and the deviation on the Hammett plot might not be a consequence of the product having a different composition or structure. The solved structure is shown in Figure 5. Comparison with the crystal structure of the monomeric adduct with pyridine[19] shows that this is not so. The two structures are analogous; the Re−N distances are very similar in the two structures, 215.3 and 214.9 pm. The rhenium atom exhibits a distorted trigonal bipyramidal geometry with atoms S(1), O(1), and C(1) in the equatorial plane and atoms S(2) and N in the apical positions. Atoms Re, S(1), O(1), and C(1) are coplanar within 10 pm. The angle S(2)−Re−N spans 152.68(8)°, differing significantly from linearity. As a result of the trans location of atoms S(2) and N the Re−S(2) distance, 229.95(9) pm, is longer than the Re−S(1) bond length, 228.15(9) pm, and

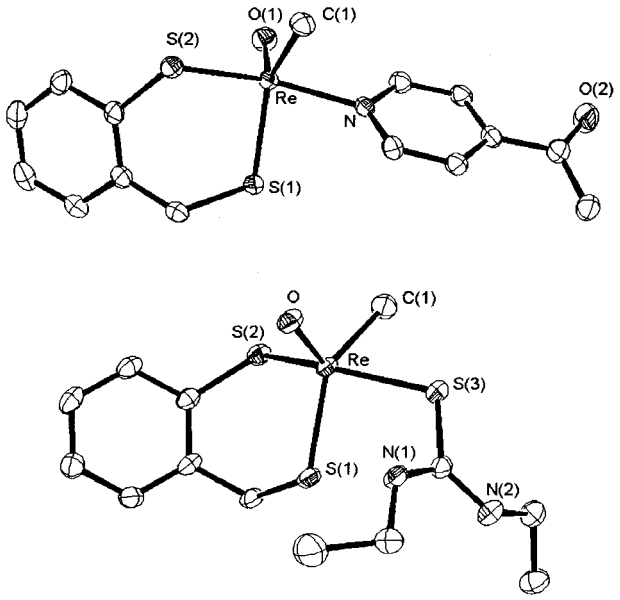

Figure 5. Top: perspective view of the monomeric 4-acetylpyridine complex **ML** with thermal ellipsoids of 50% probability level. Selected bond lengths (pm) and angles (deg) are the following: Re−O(1), 168.6; Re−C(1), 210.9; Re−N, 215.3; Re−S(1), 228.2; Re−S(2), 230.0; O(1)−Re−N, 99.90; C(1)−Re−N, 81.57; S(1)−Re−N, 82.20; S(2)−Re−N, 152.68. Bottom: perspective view of the monomeric 1,3-diethylthiourea complex **ML** with thermal ellipsoids of 50% probability level. Selected bond lengths (pm) and angles (deg) are the following: Re−O, 169.8; Re−C(1), 214.5; Re−S(1), 229.7; Re−S(2), 232.5; Re−S(3), 237.24; O−Re−S(3), 105.50; C(1)−Re−S(3), 78.96; S(1)−Re−S(3), 86.58; S(2)−Re−S(3), 148.71.

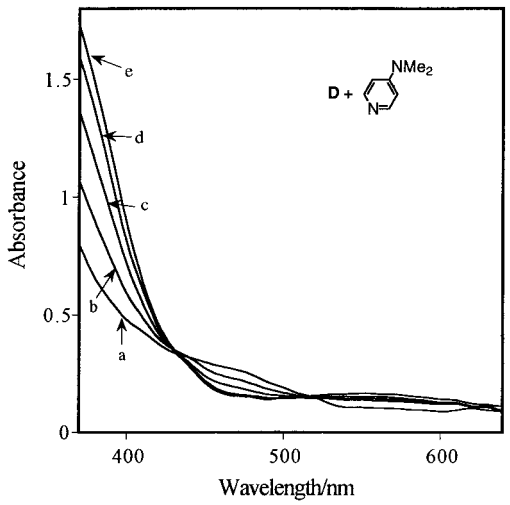

Figure 6. UV−vis spectra recorded 1.0 ms after mixing **D** with 4-(dimethylamino)pyridine. Each spectrum was constructed using the first reliable absorbance readings from 29 independent stopped−flow kinetic traces at a 10 nm wavelength interval. Initial concentrations in mmol L^{-1} are the following: [**D**] = 0.408 for all spectra; [4-Me2N−Py] = 0 (a), 2.51 (b), 6.89 (c), 13.8 (d), 27.6 (e) at 25.0 °C in benzene.

the difference is statistically significant. However, both distances are well within the typical range for rhenium−sulfur single bonds. The rhenium−oxygen and rhenium−carbon bond lengths are in good agreement with corresponding parameters in similar complexes.

The 2-substituted pyridine derivatives were found to be less reactive and led to reactions in which the equilibrium in eq 2 lay more toward **D**, most probably because of steric hindrance. That is, the interaction with the rhenium atom of the fairly crowded **D** is disfavored. Addition of a 100-fold excess of 2-picoline (2-methylpyridine) was not enough to monomerize **D** completely. Only k_a contributed significantly to the rate; its value is given in Table 1. Consistent with that, treatment of **D** with excess 2,6-lutidine (2,6-dimethylpyridine), 2,6-di-*tert*-butyl-4-methylpyridine, or 2-phenylpyridine gave no evidence for monomerization.

4-(Dimethylamino)pyridine, DAP, an extremely nucleophilic pyridine derivative, gave the usual green color with **D** in a reaction that was complete even at the lowest concentrations. *N*,*N*-Dimethylaniline, on the other hand, did not react with **D**, leading us to conclude that the nitrogen in the pyridine ring of DAP is the one coordinated to rhenium forming **M**−DAP, as with the other pyridine derivatives. Monomerization of **D** with DAP could be followed only by the stopped−flow technique. An initial and very rapid (τ < 1 ms) reaction was noted within the mixing time. The accompanying initial absorbance jump provided evidence for the significant formation of **D**−DAP in a fast equilibrium step. The corresponding spectra are shown in Figure 6. The analysis of the data according to eq 3 afforded the value $K_1 = 126 \pm 3$ L mol^{-1} based on a global fit. The data collected during the subsequent kinetics stage of the reaction followed first-order kinetics. The values of k_{obs} for monomerization varied with [DAP] according to the following rate law:

$$\frac{d[\mathbf{ML}]}{dt} = 2\frac{k_b[\mathbf{L}]^2}{1 + K_1[\mathbf{L}]}[\mathbf{D}] \qquad (14)$$

The rate constant k_b was determined with K_1 fixed at its value known from the equilibrium measurements. Least-squares fitting gave $k_b = (6.41 \pm 0.03) \times 10^4$ L^2 mol^{-2} s^{-1}.

Pyrazine and 4-methylthiazole were also used in monomerization studies. They gave the same rate law as pyridine derivatives. The rate constants are listed in Table 1. Both ligands are included in Figure 1, illustrating the linear free energy relationship. The value of k_b for 4-methylthiazole is the only datum that deviates significantly from the line defined by the pyridine derivatives. This can be explained by the fact that 4-methylthiazole is substituted on the ring carbon next to the nitrogen. Thus, steric effects may also influence its reaction, especially the pathway involving $\mathbf{DL}_2$, in which there are two ligands in the transition state.

Attempts were made to study the kinetics of the reverse reaction by adding a strong acid that would protonate free ligand, causing the reversal of eq 2. Experiments were carried out with 4-picoline in which excess trifluoromethanesulfonic acid was added to a solution of the monomeric 4-picoline complex. The green color of the monomer diminished, and the yellow color of the dimer reappeared in some hours. The system was not quite ideal for kinetic studies owing to the limited miscibility of benzene and trifluoromethanesulfonic acid. However, meaningful but limited kinetics data could be obtained by UV−vis spectrophotometry. The data gave a reasonable fit to an integrated second-order rate equation, and the second-order rate constant was estimated to be ∼0.15 L mol^{-1} s^{-1}. This gives a kinetic estimate of the equilibrium constant for monomerization of $K_D \approx 0.89 \times 10^3$ L mol^{-1}, in good agreement with the value of 1.0×10^3 L mol^{-1} found in equilibrium studies.

Triarylphosphines. With these ligands the monomerization reactions proceeded to completion even at the smallest concentrations applicable. The rate law given in eq 9 was confirmed for every derivative. The rate constants are summarized in Table 2 and are plotted against the Hammett σ value in Figure 7. The ρ value is −1.26 for k_a and −1.89 for k_b, with respective correlation coefficients of 0.934 and 0.992.

Table 2. Kinetic Data for Monomerization with Triarylphosphines and Other Ligands at 25.0 °C in Benzene

	3σ	k_b/L^2 mol^{-2} s^{-1}	k_a/L mol^{-1} s^{-1}
$(4\text{-}XC_6H_4)_3P$, X =			
CH_3O	−0.81	$(4.35 \pm 0.03) \times 10^1$	$(1.29 \pm 0.04) \times 10^{-1}$
CH_3	−0.51	$(1.35 \pm 0.05) \times 10^0$	$(7.0 \pm 0.2) \times 10^{-2}$
H	0.00	$(5.1 \pm 0.6) \times 10^{-2}$	$(1.57 \pm 0.05) \times 10^{-2}$
F	0.18	$(1.1 \pm 0.2) \times 10^{-2}$	$(4.1 \pm 0.2) \times 10^{-3}$
Cl	0.69	$(1.3 \pm 0.3) \times 10^{-2}$	$(2.2 \pm 0.2) \times 10^{-3}$
CF_3	1.62	$(4.0 \pm 1.2) \times 10^{-4}$	$(1.2 \pm 0.2) \times 10^{-4}$
$(Me_2N)_2CS$		8.6 ± 0.7	$(2.4 \pm 0.1) \times 10^{-1}$

Tris(*p*-methoxyphenyl)phosphine gave rise to an intermediate that was detected by spectrophotometry and NMR. It is proposed to be an isomer of **ML**, designated **ML***. The concentration of this intermediate remains low throughout the process. Its characteristics could be studied much better from exchange reactions and will be dealt with in that section. It is postulated that **ML*** is the immediate product of monomerization in every reaction between **D** and triphenylphosphine derivatives, but it undergoes isomerization to give **ML** in a process that is fast relative to the monomerization itself.

Ligand-Catalyzed Monomerization. As explained in the preceding sections, triarylphosphines are thermodynamically favored over pyridine complexes, the phosphines being stronger Lewis bases, whereas pyridines are favored kinetically. It seemed possible, therefore, that pyridine might catalyze the formation of **M**−PPh_3. Experiments were therefore done starting with **D**, Ar_3P, and (added initially or mid-course) Py. Figure 8 depicts the results from such an experiment. Without pyridine, **M**−PPh_3 forms slowly; at the point where pyridine was added, its buildup rate accelerated sharply.

Matrix rank analysis of time-resolved UV−vis spectra (some of which are given in Figure 21 of Supporting Information) indicated the presence of only two absorbing species throughout the time course; they were the dimer and the monomeric phosphine complex; the monomeric pyridine complex was too fleeting. The positions of the isosbestic points of the **D** + PPh_3 reaction did not change after the addition of pyridine. This conclusion was further affirmed by NMR experiments in which only the signals corresponding to the **D** and **M**−PPh_3 were detected. The rate law confirmed for this reaction exhibits a mixed term that is first-order with respect to each of triphenylphosphine and pyridine:

$$\frac{d[\mathbf{M}-PPh_3]}{dt} = 2k_{mixed}[\mathbf{D}][Py][PPh_3] \qquad (15)$$

This rate law implies the intervention of a **DLL′** complex with two different ligands. Other terms that apply to the separate reactions of PPh_3 and Py separately proved to be negligible with respect to the mixed term, in particular,

$$k_{mixed}[Py][PPh_3] \gg k_b^{Py}[Py]^2 > k_a^{PPh3}[PPh_3] + k_b^{PPh3}[PPh_3]^2 \qquad (16)$$

The value $k_{mixed} = 37.1 \pm 0.6$ L^2 mol^{-2} s^{-1} was determined. **M**−Py was not detected because it reacted immediately with triphenylphosphine to give **M**−PPh_3 (see a later section about this reaction studied directly). We suggest, therefore, that these steps occur:

$$\mathbf{D} + \mathbf{L} + \mathbf{L}' = \{\mathbf{DLL}'\} \rightarrow \mathbf{M}-PPh_3 + \mathbf{M}-Py$$

$$\mathbf{M}-Py + PPh_3 \rightarrow \mathbf{M}-PPh_3 + Py$$

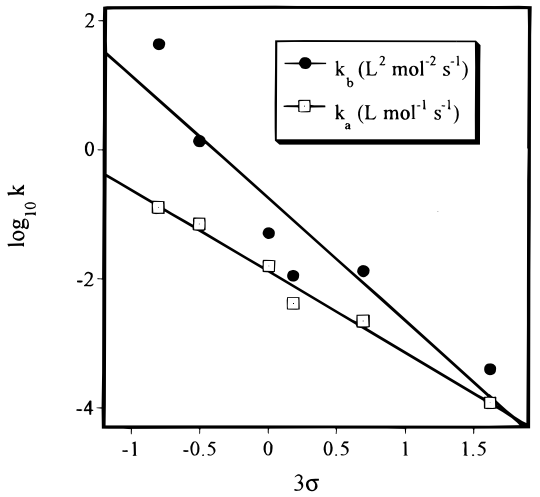

Figure 7. Hammett plot for the kinetics of monomerization reaction between **D** and triarylphosphines, $(XC_6H_4)_3P$. Rate constants were determined in benzene at 25.0 °C.

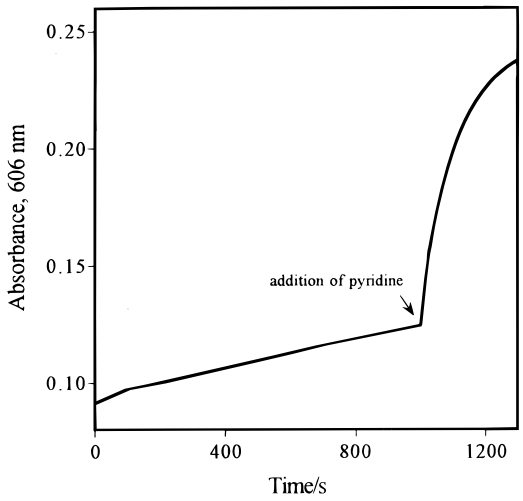

Figure 8. Sample kinetic curve to demonstrate the catalytic effect of pyridine in the monomerization of **D** with triphenylphosphine. A defined amount of pyridine was added at one time during the experiment. Initial concentrations are the following: [**D**] = 0.508 mmol L^{-1}; [PPh_3] = 14.4 mmol L^{-1}; [Py] = 9.9 mmol L^{-1} after injection; 25.0 °C, benzene.

The second step was confirmed directly, as presented in a subsequent section. It is indeed more rapid than the mixed-ligand process, consistent with our failure to detect **M**−Py during these experiments.

Other Neutral Ligands. No reaction of the dimer was detected with diethyl ether, tetrahydrofuran, propylene oxide, 1,1,3,3-tetramethylurea, acetone, triphenylphosphine oxide, triphenylphosphine sulfide, triphenylarsine, ethyl thiocyanate, thiophene derivatives, and acetonitrile. Reaction of *n*-butyl isocyanide gave a mixture of at least five products, none of which was identified.

The crystal structure of **ML** with **L** = 1,1,3,3-tetramethylthiourea (Me_4tu) was reported earlier.[19] The rate law governing the reaction between **D** and Me_4tu is given by eq 9, with $k_a = (2.4 \pm 0.1) \times 10^{-1}$ L mol^{-1} s^{-1} and $k_b = 8.6 \pm 0.7$ L^2 mol^{-2} s^{-1}. The crystal structure of the monomer with 1,3-diethylthiourea was also determined. An ORTEP view of the structure is shown in Figure 5. The monomeric complex also possesses a distorted trigonal pyramidal geometry about the rhenium atom. Atoms S(1), O, and C(1) define the equatorial plane with the rhenium atom being within 2 pm from this plane. The apical

positions are occupied by atoms S(2) and S(3) with the S(2)−Re−S(3) angle spanning 148.71(3)°. As in the previous case, this angle differs considerably from 180°, making the coordination environment of the rhenium atom intermediate between trigonal bipyramidal and square pyramidal. The rhenium−sulfur, rhenium−oxygen, and rhenium−carbon bond distances are within the ranges for corresponding bond lengths. As expected, the trans bonds Re−S(2), 232.50(7) pm, and Re−S(3), 237.24(8) pm, are noticeably longer than the equatorial Re−S(1) bond, 229.73(7) pm. All three rhenium−sulfur bonds are statistically different.

Dimethyl sulfoxide (DMSO) and 4-picoline-*N*-oxide were also confirmed to monomerize **D**. However, further reactions ensue following monomerization that involve the oxidation of Re(V) to Re(VII), thus giving MTO as a final product. These redox reactions are not relevant to the present topic and constitute a topic in their own right, which will be reported separately.

The crystal structure for the **DL** intermediate with **L** = DMSO was published earlier.[18] The formation of **DL** occurred too rapidly to be measured even by stopped−flow techniques, and so $k_1 > 3 \times 10^5$ L mol^{-1} s^{-1} was concluded. Spectrophotometric and NMR determinations gave $K_1 = 120 \pm 6$ L mol^{-1}. Evaluation of K_1 at different temperatures gave $\Delta H_1^\circ = -35.6 \pm 0.8$ kJ mol^{-1} and $\Delta S_1^\circ = -80 \pm 3$ J K^{-1} mol^{-1}.[18]

The experimentally confirmed rate law for the kinetic phase of the reaction is

$$\frac{d[\mathbf{M}-\mathbf{L}]}{dt} = 2\frac{k_d[\mathbf{L}]}{1 + K_d[\mathbf{L}]}[\mathbf{D}] \qquad (17)$$

Because K_1 is known independently for this system from 10.0 to 60.0 °C, it can be shown that very little **D** remained uncomplexed even at the lowest DMSO concentration used in the kinetic measurements displayed in Figure 10. Thus, the inequality $1 \ll K_1[\mathbf{L}] + K_1K_2[\mathbf{L}]^2$ applies. Setting $k_3 \ll k_4K_2[\mathbf{L}]$ in eq 7 converts it into another limiting form that agrees with eq 17. According to that, $k_d = k_4K_2$ and $K_d = K_2$. Consequently, $K_2 = 0.60 \pm 0.04$ L mol^{-1} and $k_4 = (9.5 \pm 0.5) \times 10^{-4}$ s^{-1} were determined at 50.0 °C in benzene. A higher temperature was used in this case because the reaction was inconveniently slow at lower temperatures.

4-Picoline-*N*-oxide gave results very similar to those of DMSO, the only difference being the time scale of the reaction. The initial absorbance readings from stopped−flow experiments, prior to the kinetic phase, were used to determine the stability constant of **DL**, $K_1 = (4.1 \pm 0.3) \times 10^3$ L mol^{-1}. From the kinetics, and eq 17, $K_2 = (1.7 \pm 0.1) \times 10^2$ L mol^{-1} and $k_4 = (5.2 \pm 0.3) \times 10^{-2}$ s^{-1} were determined.

Anionic Ligands. Tetrabutylammonium salts are usually reasonably soluble in benzene, and thus we carry out monomerization studies with a series of anionic ligands. No monomerization was detected with weakly coordinating, nonbasic anions such as trifluoromethanesulfonate, hexafluorophosphate, and tetrafluoroborate. Perrhenate ion (ReO_4^-) and tetrathioperrhenate ion (ReS_4^-) did not react with the dimer either. As reported for chloride earlier,[19] halide ions gave green products upon reaction with the yellow dimer solution. First-order kinetic curves with rate constants independent of the halide ion concentration were recorded when the halide ion was in excess over the dimer. Investigation of the spectra obtained immediately after mixing revealed stoichiometric formation of $\mathbf{DL}^-$ (see Figure 11 in Supporting Information). The species with two halides, $\mathbf{DL}_2^{2-}$, was not detected owing to the strong electrostatic repulsion between negatively charged $\mathbf{DL}^-$ and $\mathbf{L}^-$ in the nonpolar solvent benzene. The value $K_1 > 5 \times 10^4$ L mol^{-1} was estimated as a lower limit. The experimental rate law for ligand excess is

Chart 2

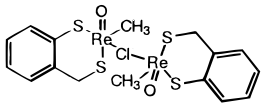

Table 3. Rate Constants for the Monomerization with Halides at 25.0 °C in Benzene

halide ion	k_3/s^{-1}
Cl^-	$(3.87 \pm 0.04) \times 10^{-4}$
Br^-	$(1.10 \pm 0.07) \times 10^{-3}$
I^-	$(1.7 \pm 0.1) \times 10^{-3}$

$$\frac{d[\mathbf{M}-\mathbf{L}]}{dt} = 2k_c[\mathbf{D}] \qquad (18)$$

Setting $K_1[\mathbf{L}] \gg 1 + K_1K_2[\mathbf{L}]^2$ and $k_3 \gg k_4K_2[\mathbf{L}]$ in eq 7 gives this limiting rate law with $k_c = k_3$. This equation is mathematically correct even without a large excess of the ligand. The rate constants determined for halide ions are given in Table 3. Activation parameters for k_3 with chloride are $\Delta H^\ddagger = 79.9 \pm 0.4$ kJ mol^{-1} and $\Delta S^\ddagger = -43 \pm 1$ J K^{-1} mol^{-1}.[19]

With thiocyanate ion stoichiometric formation of $\mathbf{DL}^-$ was also confirmed. However, the initial absorbance readings and the kinetics indicated that $\mathbf{DL}_2^{2-}$ was equilibrated with $\mathbf{DL}^-$ and $\mathbf{L}^-$ during the time of mixing (Figures 23 and 24 in Supporting Information). The experimental rate law with **L** in large excess this time is

$$\frac{d[\mathbf{ML}]}{dt} = 2\frac{k_c + k_d[\mathbf{L}]}{1 + K_d[\mathbf{L}]}[\mathbf{D}] \qquad (19)$$

This is another limiting form of eq 7 under conditions where $1 \ll K_1[\mathbf{L}] + K_1K_2[\mathbf{L}]^2$, $k_c = k_3$, $k_d = k_4K_2$, and $K_d = K_2$. Similar to the halide ions, $K_1 > 5 \times 10^4$ L mol^{-1} can be claimed, the remaining constants being $K_2 = (1.3 \pm 0.3) \times 10^2$ L mol^{-1}, $k_3 = (3.2 \pm 0.5) \times 10^{-1}$ s^{-1}, and $k_4 = 1.3 \pm 0.3$ s^{-1}.

Detailed experiments were also carried out in the chloride ion system with **D** in excess. Matrix rank analysis of time-resolved spectra recorded in several different kinetic experiments gave the number of absorbing species as 4, in contrast to the expected value of 3 (**D**, **D**−Cl^-, and **M**−Cl^-). Indeed, a new set of ^{1}H NMR signals was seen when **D** was in stoichiometric excess over chloride. The new species is proposed to be a chloro bridged dimer $\{\mathbf{M}-Cl-\mathbf{M}\}^-$, an isomer of **D**−$Cl^-$, without sulfur bridges so that its spectroscopic properties are more similar to those of the monomeric complexes. The proposed structure is shown in Chart 2; the equivalency of the benzylic protons requires a species more symmetric than, for example, one with one S and Cl bridging groups.

Ligand Exchange with Monomeric Complexes. Separate, sharp NMR signals were seen for the free and complexed ligand in any monomerization reaction. This observation shows that the ligand exchange between **ML** and free **L** is slow on the NMR time scale. To study a reaction very close to true exchange (an identity), a pseudo-exchange was created with the monomeric complex with pyridine (**L**) and excess 4-methylpyridine (**L′**):

$$\mathbf{ML} + \mathbf{L}' = \mathbf{ML}' + \mathbf{L} \qquad (20)$$

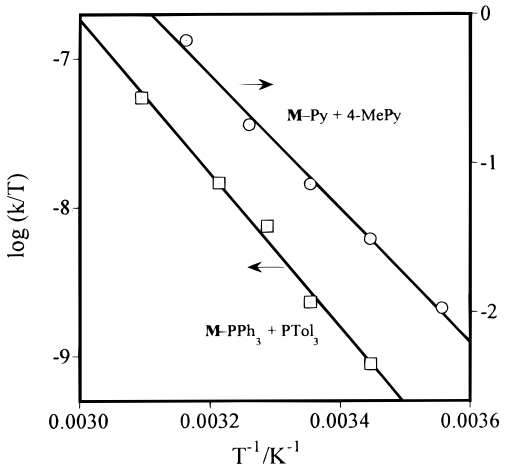

Figure 9. Temperature dependence of the rate constants in the exchange reactions **ML** + **L′** with **L** = pyridine and **L′** = 4-methylpyridine; **L** = triphenylphosphine and **L′** = tri(*p*-tolyl)phosphine.

Small differences in the spectra of the monomeric adducts made it possible to study the kinetics of the reaction with the stopped−flow technique. The following rate law was confirmed:

$$\frac{d[\mathbf{ML'}]}{dt} = k_+[\mathbf{ML}][\mathbf{L'}] - k_-[\mathbf{ML'}][\mathbf{L}] \qquad (21)$$

The values $k_+ = 95 \pm 2$ L mol^{-1} s^{-1} and $k_- = 19 \pm 6$ L mol^{-1} s^{-1} were determined by least-squares fitting. The equilibrium constant for reaction 20, $K_{ex} = [\mathbf{ML'}][\mathbf{L}]/([\mathbf{ML}][\mathbf{L'}])$ could be estimated in three independent ways. First, K_{ex} could be calculated from the data given in Table 1 as the square root of the ratio of the K_D values for **ML′** and **ML**, giving $K_{ex} = 2.4 \pm 0.1$. Second, direct fitting to the equilibrium absorbance readings in reaction 20 resulted in $K_{ex} = 2.0 \pm 0.3$. Finally, from kinetics, $K_{ex} = k_+/k_- = 5.0 \pm 2.5$. The high standard deviation of the kinetic value reflects the high uncertainty in k_-, although the agreement among these three values is acceptable. A preferable value of k_- can be obtained from k_+/K_{ex}, which gives 40 ± 4 L mol^{-1} s^{-1}.

The temperature-dependent values of k_+ are shown in Figure 9, plotted according to the Eyring equation. The activation parameters were determined as $\Delta H^{\ddagger} = 36 \pm 2$ kJ mol^{-1} and $\Delta S^{\ddagger} = -85 \pm 7$ J K^{-1} mol^{-1} (8−43 °C). The large negative value for the activation entropy suggests an associative I_a pathway for this process.

The same experiments were done with triphenylphosphine (**L**) and tri(*p*-tolyl)phosphine (**L′**) as well. This exchange was much slower. The rate law given in eq 20 was confirmed, and $k_+ = 0.053 \pm 0.003$ L mol^{-1} s^{-1} and $k_- \approx 0.02$ L mol^{-1} s^{-1} were determined. Their ratio gives $K_{ex} \approx 2.5$, a value that is consistent with the equilibrium absorbance readings. The temperature dependence of k_+ is shown in an Eyring equation format in Figure 9. $\Delta H^{\ddagger} = 41 \pm 2$ kJ mol^{-1} and $\Delta S^{\ddagger} = -132 \pm 6$ J K^{-1} mol^{-1} (17−50 °C). The activation entropy is also negative in this case; its value is even larger than for the analogous pyridine reaction. Pyridine had a considerable catalytic effect on phosphine exchange (Figure 17 in Supporting Information). The mechanism of this catalytic reaction was found to be surprisingly complex and is not reported here.

Exchange with **L** = pyridine and **L′** = triphenylphosphine was also studied. Biphasic kinetic curves were recorded; a typical experiment on dual time bases is shown in Figure 10. The two steps were separated enough to be handled independently, however. In the first step triphenylphosphine replaces

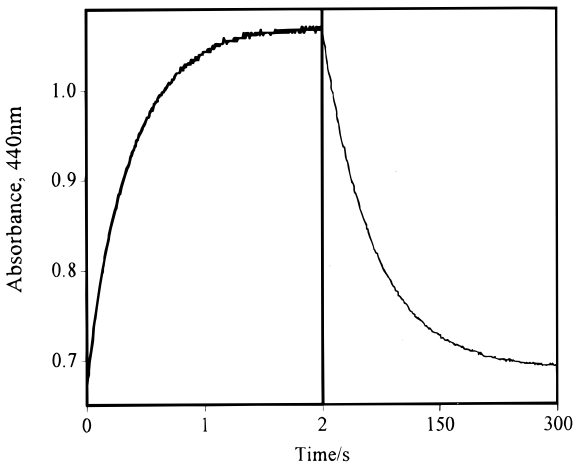

Figure 10. Sample kinetic curve in the exchange reaction between **ML** (1.15 mmol L^{-1}) and **L′** in solutions containing 17.9 mmol L^{-1} **L** (pyridine) and 25.7 mmol L^{-1} **L′** (triphenylphosphine). Conditions are in benzene at 25.0 °C. The rising portion of the curve represents the pyridine-catalyzed formation of **M**−PPh$_3$*, and the slower, falling part represents its conversion to the stable **M**−PPh$_3$ in a reaction that is also pyridine-catalyzed.

pyridine to give an **M**−PPh$_3$*, an isomer of **M**−PPh$_3$. This isomer has a UV−vis spectrum and ^{1}H and ^{31}P NMR resonances different from that determined for **M**−PPh$_3$ in independent studies (see Table 5 in Supporting Information for details). Isomerization of **M**−PPh$_3$* follows in which **M**−PPh$_3$ is produced. This isomerization is catalyzed by pyridine. The following scheme was confirmed to interpret the kinetic data:

$$\mathbf{M}\text{−Py} + \text{PPh}_3 \underset{k_{-5}}{\overset{k_5}{\rightleftharpoons}} \mathbf{M}\text{−PPh}_3\text{*} + \text{Py} \qquad (22)$$

$$\mathbf{M}\text{−Py} + \text{PPh}_3 \xrightarrow{k_6} \mathbf{M}\text{−PPh}_3 + \text{Py} \qquad (23)$$

$$\mathbf{M}\text{−PPh}_3\text{*} + \text{PPh}_3 \xrightarrow{k_7} \mathbf{M}\text{−PPh}_3 + \text{PPh}_3 \qquad (24)$$

The values $k_5 = 88.0 \pm 0.8$ L mol^{-1} s^{-1} and $k_{-5} = 16.1 \pm 0.8$ L mol^{-1} s^{-1} were determined from the kinetic analysis of the first step, giving the equilibrium constant for reaction 22 because K_5 (or K_{22}) $= k_5/k_{-5} = 5.5 \pm 0.3$. This equilibrium constant was used in the evaluation of the second step, and the remaining rate constants were resolved as $k_6 = 6.27 \pm 0.09$ L mol^{-1} s^{-1} and $k_7 = 0.2 \pm 0.1$ L mol^{-1} s^{-1} (see Supporting Information for details). It can be seen that reaction 24 plays but a marginal role in the isomerization of **M**−PPh$_3$*. Adding the unassisted first-order isomerization reaction **M**−PPh$_3$* → **M**−PPh$_3$ to the scheme given in eq 22−24 did not improve the fit at all, whereas substituting this first-order step for reaction 24 resulted in a somewhat inferior fit.

It was also possible to estimate the overall equilibrium constant for this exchange. This equilibrium constant is defined as $K_6 = [\mathbf{M}\text{−PPh}_3][\text{Py}]/([\mathbf{M}\text{−Py}][\text{PPh}_3])$. The value obtained from NMR based on integration of signals is $K_6 = 930 \pm 30$, whereas UV−vis gave $K_6 = 860 \pm 20$. Evaluating the two sets of results together gave $K_6 = 900 \pm 50$.

Discussion

The steps for dimer and ligand reactions represented by k_1 and k_2 are assumed to be very rapid for all the ligands. This was explicitly proved for those ligands with which **DL** attains a detectable concentration (for DMSO,[18] 4-pyridine-*N*-oxide,

4-(dimethylamino)pyridine, and halide and thiocyanate ions). In each of these cases, the reaction occurred too rapidly for the stopped−flow method. We thus infer that no significant structural rearrangement occurs around the rhenium center during that step of the reaction. The confirmed fact that the reaction **D** + **L** = **DL** is extremely fast renders it implausible to assign the reaction between **DL** + **L** as a rate-controlling step in monomerization, which would be equivalent to omitting the equilibrium formation of $\mathbf{DL}_2$. Kinetic results with **L** = DMSO, picoline-*N*-oxide, and thiocyanate also require $\mathbf{DL}_2$ as an intermediate; only small UV−vis spectral changes for the conversion of **DL** to $\mathbf{DL}_2$ were seen for these ligands.

The rate constants for monomerization with pyridine derivatives containing electron-withdrawing substituents in the para position (4-cyano, 4-acetyl, 4-formyl) show significant deviation from other pyridine derivatives on Hammett plots. The basicity of pyridine derivatives in nitromethane[21] showed the same kind of deviation when plotted against the usual Hammett σ values (Figure 18 in Supporting Information). Thus, the usual Hammett σ values do not seem to be applicable for pyridine derivatives containing electron-withdrawing substituents in the para position.

Kinetics results on re-dimerization following the addition of triflic acid suggest that two **M**−Py molecules associate to give a dimer before liberating pyridine rather than dissociation of **M**−Py into Py and **M**. This is in agreement with the microscopic reverse of monomerization, showing that the acid has not opened a new pathway. It can also be concluded that the possible reaction $\mathbf{M}-\mathrm{Py} + \mathrm{H}^+ \rightarrow \mathbf{M} + \mathrm{HPy}^+$ has no significance. Most probably such a step would be thermodynamically unfavorable in that the rate of pyridine exchange suggests that it should be reasonably fast if the reaction were thermodynamically allowed. Similar re-dimerization experiments with less reactive pyridine derivatives may have given some information on **M** itself. Unfortunately, these experiments were not feasible owing to the limited solubility of triflic acid in benzene.

The large negative activation entropies determined for ligand-exchange reactions of monomeric complexes indicate that **M** is not a likely intermediate in these reactions either. The transition state most probably contains a six-coordinated Re(V) center. This fact is seen as further evidence to prove that the dissociation of **ML** into **L** and **M** is unimportant.

Efforts to crystallize anionic derivatives were unsuccessful. Chloride is known to bridge between rhenium centers in earlier examples,[22] giving some support to a postulated $\mathbf{M}-\mathrm{Cl}-\mathbf{M}^-$ structure. The NMR and UV−vis spectroscopic properties of the proposed $\mathbf{M}-\mathrm{Cl}-\mathbf{M}^-$ are much closer to those of $\mathbf{M}-\mathrm{Cl}^-$ than to $\mathbf{D}-\mathrm{Cl}^-$. Unlike the halides, the kinetic role of $\mathbf{DL}_2^{2-}$ was confirmed with thiocyanate. Its formation constant could also be determined. This reflects the well established fact that thiocyanate usually forms much more stable complexes than halides. So formation of $\mathbf{DL}_2^{2-}$ is possible with thiocyanate despite the electronic repulsion that represses this process with the halides. It should also be noted that tetrabutylammonium thiocyanate is considerably more soluble in benzene than tetrabutylammonium halides, so higher ligand concentrations could be used favoring the formation of $\mathbf{DL}_2^{2-}$.

The structure of the $\mathbf{M}-\mathrm{PPh_3}$* species remains unclear. ^{1}H NMR and ^{31}P NMR show without doubt that it has the same composition as $\mathbf{M}-\mathrm{PPh_3}$. However, any investigation other than NMR or UV−vis spectroscopy has not proved feasible because the lifetime of the species is about 2−3 min at room temperature. A geometric isomer must be considered, since the two S atoms of the dithiolate are inequivalent; we plan to study this further.

$K_6 = 900$ was determined from exchange studies. One can but assume that monomerization reactions of triarylphosphines are also equilibrium reactions, with a K_D (PAr_3). One can calculate a value for triphenylphosphine from the relation

$$K_D^{PPh_3} = K_D^{Py} K_6 \qquad (25)$$

giving 1.6×10^5 L mol^{-1}. This value implies an almost complete reaction under the accessible conditions and could not be determined directly because of the experimental difficulties connected with slow equilibration, especially at the very low phosphine concentrations needed to obtain a balanced system. On the basis of the data presented in this paper, it can be estimated that several weeks might be needed to reach a detectable true equilibrium in the reaction of **D** with PPh_3.

On the basis of the value of K_6, it is also possible to calculate the equilibrium constant for the isomerization of $\mathbf{M}-\mathrm{PPh_3}$* to $\mathbf{M}-\mathrm{PPh_3}$; $K_{iso} = [\mathbf{M}-\mathrm{PPh_3}]/[\mathbf{M}-\mathrm{PPh_3}^*] = K_6/K_5 = 164$. This value is consistent with the fact that only $\mathbf{M}-\mathrm{PPh_3}$ is detected in equilibrium.

The oxo-bridged Re(V) dimer $\{Cp^*Re(O)\}_2(\mu\text{-}O)_2$, reported by Gable,[23] provides an informative comparison. The reaction of that dimer with styrene oxide was studied by quantitative kinetics. It was found to proceed via the corresponding monomeric form, and a monomer−dimer equilibrium was established. No signs of such an equilibrium between **D** and its monomer **M** were seen even at the highest temperatures and concentrations applicable, giving a lower limit for the dimerization equilibrium constant $K = [\mathbf{D}]/[\mathbf{M}]^2 > 10^7$ L mol^{-1}. It is assumed that **M** reacts very rapidly with ligands because it could not be detected (i.e., its concentration was lower than 10^{-6} mol L^{-1}) in our studies. Coordination of a ligand to one of the metal centers of $\{Cp^*Re(O)\}_2(\mu\text{-}O)_2$ seems to be less likely because the electron count of its Re is 18, in contrast with the electron count of 14 for Re in **D**. This suggests why the reactions of $\{Cp^*Re(O)\}_2(\mu\text{-}O)_2$ are predominantly dissociative (D), whereas they are associative (A) for **D**.

Acknowledgment. This research was supported by the National Science Foundation. G.L. also thanks the U.S.−Hungary Science and Technology Program for financial support. Some of this research was carried out in the facilities of the Ames Laboratory. Three anonymous reviewers are also acknowledged for their useful suggestions.

Supporting Information Available: Graphs and tables containing additional kinetic and spectroscopic data referred to in the text, detailed description of the kinetic equations used to obtain rate constants with less reactive pyridine derivatives, and X-ray crystallographic tables. X-ray crystallographic data files for the monomeric complexes **ML** with **L** = 4-acetylpyridine and diethylthiourea in CIF format. This material is available free of charge via the Internet at http://pubs.acs.org.

IC991431P

(21) Korolev, B. A.; Osmolovskaya, L. A.; Dyumaev, K. M. *Zh. Obshch. Khim.* **1979**, *49*, 898−904.
(22) Dunbar, K. R.; Powell, D.; Walton, R. A. *Inorg. Chem.* **1985**, *24*, 2842−2846.
(23) Gable, K. P.; Juliette, J. J. J.; Gartman, M. A. *Organometallics* **1995**, *14*, 3138−3140.